A 5200-year Paleoecological and Geochemical Record of Coastal Environmental Changes and Shoreline Fluctuations in Southwestern Louisiana: Implications for Coastal Sustainability

Qiang Yao[1]*, Kam-biu Liu[1], Alejandro Antonio Aragón-Moreno[1], Erika Rodrigues[2], Y. Jun Xu[3], Nina S. Lam[4],

[1] Department of Oceanography and Coastal Sciences, College of the Coast and Environment, Louisiana State University, Baton Rouge, LA 70803

[2] Laboratory of Coastal Dynamics, Graduate Program of Geology and Geochemistry, Brazil Federal University of Pará, Belém (PA), Brazil.

[3] School of Renewable Natural Resources, Louisiana State University, Baton Rouge, LA 70803

[4] Department of Environmental Sciences, Louisiana State University, Baton Rouge, LA 70803

*Corresponding author:

Qiang Yao

Department of Oceanography and Coastal Sciences, Louisiana State University, 93 South Quad Drive, Baton Rouge, LA 70803

qyao4@lsu.edu

Highlights:

- Louisiana's Chenier Plain was strongly influenced by the Mississippi-Atchafalaya River course changes.
- Coastal ecosystems changed from swamp to maritime forest during 5200-3440 cal yr BP, and from swamp to marsh to beach/dune community after 3440 cal yr BP.
- Shoreline retrogradation began at ~3440 cal yr BP as the Mississippi River outlet switched from west to east.
- Holocene shoreline fluctuations of the Chenier Plain were tied to the Mississippi River Delta Switch and relative sea level rise.

Keywords: Coastal morphodynamics, Palynology, Shoreline fluctuations, Mississippi River Delta Switch, Louisiana Chenier Plain, Holocene

1. Introduction

Coastal wetlands provide many essential ecological services to coastal communities. Particularly, in the state of Louisiana, wetlands are a vital natural resource because Louisiana has the largest contiguous wetland system in the lower 48 states and contains over 40% of the wetlands in the continental U.S. (Couvillion and Beck, 2013). However, since the 1930s, almost 5000 km^2 of wetlands have disappeared from the Louisiana coastlines, accounting for ~90% of the total coastal wetland loss in the continental U.S. (Couvillion et al., 2011, 2017). Particularly during the peak of wetland loss between 1970s and 1980s, an area of wetlands equivalent to the size of a football field disappeared every hour (Couvillion et al., 2011). This rapid wetland loss is caused by a combination of human and natural processes, such as hydrology alteration, landscape fragmentation, coastal excavation, subsidence, sea level rise, and hurricanes (Bush et al., 2018; Lam et al., 2018a, b; Schoolmaster et al., 2018; Xu et al., 2018). Among them, the Mississippi River Delta Switch is believed to play an important role in the chronic wetland loss in Louisiana (Roberts, 1997) because the substrate of both western and eastern Louisiana coastlines was formed from sediments deposited and carried by the Mississippi River over the past 7000 years (Rosen and Xu, 2011). For every ~1000 years, the Mississippi River changed its course and caused erosion, compaction, and subsidence to the old delta lobe, subsequently reshaping the coastal morphodynamics and ecosystem development in Louisiana (Roberts, 1997; McBride et al., 2007; Owen, 2008; Rosen and Xu, 2011) (Fig. 1). During the past few decades, these natural deltaic cycles have been heavily altered by human activities, accelerating the deterioration of coastal ecosystems - an estimated net loss of 1,700 km^2 of coastal wetlands in Louisiana by 2050 (Reed and Wilson, 2004). Thus, to predict the coastal morphodynamics and ecosystem development in the future, it is essential to reveal the history of coastal wetland development in relation to the delta

switch in Louisiana since the mid-Holocene.

During recent decades, the cyclic delta-building process of the Mississippi River has been documented in a number of studies (Coleman, 1988; Roberts, 1997; Coleman et al., 1998). It is generally acknowledged that six major delta complexes (Sale-Cypremont 4600-3500 BP, Teche ~3500-2800 BP, St. Bernard ~2800-1000 BP, Lafourche ~1000-300 BP, Plaquemine-Balize 750 BP to present, Atchafalaya-Wax Lake 400 BP to present) were developed since the mid-Holocene (Roberts, 1997; Day et al., 2007; McBride et al., 2007; Kemp et al., 2016) (Fig. 1). These deltaic cycles significantly influenced the geomorphology of the Louisiana Chenier Plain, an extension of the Mississippi Deltaic Plain. The Louisiana Chenier Plain is one of the world's largest chenier plains (Schwartz, 2006) comprising an area of about 5000 km^2 with a west-east coastline of approximately 200 km stretching from approximately 29.5º N to 33.2º N and from 91.3º W to 94.0 º W (He and Xu, 2016). Previous studies have suggested that when the Mississippi River delta complex switched to a relatively western position (Sale-Cypremont and Atchafalaya-Wax Lake), the southwestern Louisiana coastlines underwent coastal progradation from renewed sediment input from the Mississippi River, forming the foundation of coastal wetlands in southwestern Louisiana (Owen, 2008). When the complex switched to farther east (Teche, St. Bernard, Lafourche, Plaquemine/Balize), coastlines experienced retrogradation and cheniers were formed because marine processes overwhelmed fluvial processes (McBride et al., 2007). Although these studies provided background datasets to study the Holocene geomorphological history of Louisiana coastlines, major gaps still exist in the paleoecological data network – the Holocene history of coastal wetland development in southwestern Louisiana has not been documented. In particular, the link between the Mississippi River Delta Switch and the southwestern Louisiana coastal morphodynamics is still unclear (Rosen and Xu, 2011).

Since the mid-Holocene, a dense layer of fluvial sediments and humic clay has deposited on the wetlands in Louisiana's Chenier Plain (Roberts, 1997; Owen, 2008), providing an ideal repository for proxy-based paleoecological, hydrological, and sedimentological reconstructions. Among different proxy methods, palynological analysis has been widely used for the reconstruction of vegetation and ecosystem development in North America (e.g., Huntley and Webb, 2012). However, well-dated palynological records are remarkably rare from coastal areas in the continental U.S. (Willard et al., 2001, 2004; Willard and Bernhardt, 2011; Van Soelen et al., 2012; Yao et al., 2015; Yao and Liu, 2018, 2017; Jones et al., 2019), and even fewer studies have documented the wetland development in Louisiana at centennial to millennial timescales (Ryu et al., 2018; Kiage, 2020). Chenier Plains are investigated in many coastal regions for their marine influences. Very little is known about the long-term impacts of alluvial sediments from the near-by rivers on chenier shoreline development and the ecosystem changes associated with it.

To fill the knowledge gap, this study utilizes a multi-proxy approach to reconstruct the sedimentary history of the Louisiana Chenier Plain and investigates chenier ecosystem changes associated with it. Our goal was to test the hypotheses that 1) the morphodynamic development of the Louisiana Chenier Plain is dominated by the Mississippi River, and 2) changes in the course and sediment supply of the Mississippi River will therefore strongly affect the physical and ecosystem development of the Chenier Plain. Specially, the study used palynological, loss-on ignition (LOI), grain-size, and X-ray fluorescence (XRF) measurements of a 525 cm sediment core (ROC-4) from the Chenier Plain at Rockefeller Wildlife Refuge (RWR) (Fig. 1) to reconstruct the Holocene history of coastal wetland development on the southwestern Louisiana coastlines in relation to the Mississippi River Delta Switch on a regional scale. The study also employed

hydrologic and remote sensing data to assess the recent development of the chenier ecosystem in light of future coastal morphodynamics and restoration strategies.

2. Research area

2.1. Study Site Description

Our study area, Rockefeller Wildlife Refuge (RWR), is a state-owned large area of marshland located at the eastern end of the Chenier Plain in Cameron and Vermillion parishes, southwestern Louisiana (Fig. 1). The RWR sits on a narrow basin with low beach barriers to the south and high ridges to the north. Before the occurrence of major landscape alterations due to human activities, precipitation and fluvial discharge from surrounding ridges drain into this basin, thus creating extensive freshwater marshes near the north side of RWR (Selman et al., 2011). Vegetation in the freshwater marsh is primarily comprised of cattail (*Typha* sp.), grasses (*Poa* sp.), and sawgrass (*Cladium* sp.). The lower two-thirds of the basin are drained by dendritic tidal channels, thus inhabiting brackish marsh in the middle of the basin and saltmarsh close to the beach. Vegetation in the lower two-thirds of the basin are dominated by *Spartina* sp., with wiregrass (*Spartina patens*) dominating the brackish marsh and iva (*Iva frutescens*), hogcane (*Spartina cynosuroides*), and cordgrass (*Spartina alterniflora*) dominating the saltmarsh (Selman et al., 2011). At the south end of RWR are beaches consisting of shells and shell fragments that become coarser landward from the shoreline (Selman et al., 2011). Some foraminifera, and few quartz and gravels fragments are also present along the beach (Yao et al., 2018). *Batis maritima*, a succulent plant commonly found in saltmarshes and beach ridges along the Gulf coastlines, occupies extensive backbarrier marshes behind the beach. The vegetation composition of the natural wetlands in RWR has been altered substantially over the past 40 years due to water

92 management and construction of levees and infrastructures (Selman et al., 2011). A recent study
93 indicates that the shoreline in RWR was retreating at a rate of ~14.5 cm/yr since 1998 (Yao et al.,
94 2018). Therefore, there is an urgent need to document the Holocene history of these coastal
95 wetlands before they are lost to shoreline retreat and coastal erosion.
96
97 *2.2. The Holocene history of the Mississippi River Delta complexes*
98 The framework of the Mississippi River Delta cycle was established in the early 1950s by
99 McIntire (1954). Based on McIntire's initial concept, the first widely used delta complexes
100 diagram was published in the late 1950s by Kolb and Van Lopik (1958). Later on, the chronology
101 of different complexes was established in the 1960s (McFarlan, 1961; Frazier, 1967). In recent
102 decades, the framework and chronology of the Delta complex-building processes have been
103 improved and reviewed by several landmark studies (Coleman, 1988; Coleman et al., 1998; 2007;
104 Kemp et al., 2016). Since the timeline of the delta cycle is defined slightly differently by various
105 authors, this study attempts to synthesize the Holocene history of the Mississippi River Delta
106 complexes based on the commonly cited studies published in recent years (Roberts, 1997; Day et
107 al., 2007; McBride et al., 2007; Kemp et al., 2016;). Our synthesis recognizes six phases in the
108 development of the Mississippi River Delta complexes: (1) Sale-Cypremont (4600-3500 BP), (2)
109 Teche (3500-2800 BP), (3) St. Bernard (2800-1000 BP), (4) Lafourche (1000-300 BP), (5)
110 Plaquemine-Balize (750 BP to present), and (6) Atchafalaya-Wax Lake (400 BP to present)
111 (Roberts, 1997; Day et al., 2007; McBride et al., 2007; Kemp et al., 2016) (Fig. 1). These
112 complexes typically turned-around at a frequency of every ~1000-2000 years, deposited
113 sedimentary profiles up to 300 cm thick on the inner shelf (Roberts, 1997).
114

3. Materials and methods

3.1 Field sampling

In 2013, a 525 cm sediment core ROC-4 (29.668935°N, 92.850490°W) was recovered from the succulent marsh ~30 meter behind the beach barrier in RWR. The elevation of the coring site was ~1 m above the sea-level at the of time of coring but submerged after 2017 due to rapid shoreline retreat. The core was retrieved by using a Russian peat borer and consisted of eleven ~50 cm-long core segments. Each of the core segment was measured, photographed, and wrapped in the field, and stored in a cold room (4°C) at the Global Change and Coastal Paleoecology Laboratory in Louisiana State University.

3.2 Laboratory analyses

In this study, grain-size analysis was performed at contiguous 20 cm interval throughout core ROC-4 by using a Malvern Mastersizer 2000 grainsize analyzer. Approximately 1 gram (dry weight) of sediments was used for each sample, and the laboratory procedures followed the standard protocols described in Zhang et al. (2019). Accordingly, the sand (63-2000 μm), silt (2-63 μm), and clay (< 2 μm) fractions were reported for each sample.

Loss-on-ignition (LOI) and X-ray fluorescence (XRF) analyses were performed at contiguous 1 cm interval throughout the core. LOI analysis reveals the % wet weight for water, and % dry weight for organics and carbonates in the sediment profile (Liu and Fearn, 2000). XRF analysis was performed by using an Olympus Innov-X DELTA Premium XRF analyzer. XRF is widely used in coastal studies and it measures the elemental concentrations (ppm) of major chemical elements in coastal sediments (e.g., Ca, Sr, and Zr) (Yao and Liu, 2017, 2018; Yao et al., 2018, 2019). Among the detected elements, only Ca and Sr showed significant and meaningful

fluctuations throughout the core and are therefore reported here.

Thirty samples were taken at 5 to 20 cm intervals for palynological analysis. Each sample consisted of 1.8 ml of sediments. All pollen samples were processed using standard laboratory procedures described in Kiage and Liu (2009) and Yao et al. (2015). One tablet of *Lycopodium* (L_c) (~20,583 spores) was added to each sample as an exotic marker to aid the calculation of pollen concentration (grains/cm^3) (sum = Lc added $*$ no. of spores counted/Lc counted/volume of sample). Pollen identification was based on published pollen keys by Chmura et al. (2006), Willard et al. (2004), and McAndrews et al. (1973). Over 300 grains of pollen and spore were counted and photographed in every sample by using an Olympus microscope at 400x magnification. Other palynomorphs, including charcoal fragments (>10 μm in size), dinoflagellates tests, and foraminifera linings were also counted. The grain-size, LOI, XRF, and pollen results are displayed in Figure 2.

3.3 Statistical analyses

Principal component analysis (PCA) was performed to reveal the distribution of pollen taxa in relation to coastal morphodynamics and ecosystem development by using the C-2 version 1.8 (standardize data by variables, center data by variables, rotate axes) on all pollen samples. The PCA provided a foundation to categorize various pollen taxa into statistically meaningful groups, which were then used to verify wetland sub-environments interpreted from the pollen dataset.

3.4 Chronology

Three samples from core ROC-4 were sent to International Chemical Analysis Inc., Florida, for AMS ^{14}C measurements (Table 1). Approximately 1 gram of sediment was used for

each ^{14}C sample. Pretreatment for each sample was performed in the Global Change and Coastal Paleoecology Laboratory at Louisiana State University by sieving the sediments with a 200 μm sieve to separate the <200 μm fine sediment fraction consisting of bulk clastic and organic sediments from the >200 μm coarse sediments fraction consisting of roots and sand (Yao et al., 2015). The fine sediment fractions were used for AMS ^{14}C measurements. More detailed information describing the pretreatment of ^{14}C samples from dynamic coastal environments is provided in supplementary content published by Yao et al. (2015). All ^{14}C dates in this study were converted into calendar years before present (BP) by Calib 7.1 (Stuiver et al., 2020), rounded to the nearest decade, and reported as calibrated year before present (cal yr BP).

4. Results

4.1 Chronology

All three AMS ^{14}C dates were deemed reliable. They were obtained at 78 cm, 403 cm, and 525 cm from the top of the core and calibrated to ~ 590, 4340, and 5190 cal yr BP after rounding to the nearest decade (Table 1). The surface (0 cm at 2013 AD) and the three ^{14}C dates were used to calculate the sedimentation rate based on linear interpolation between points. This age model suggests that the sedimentation rate from 590 cal yr BP to the present was 1.19 mm/yr; the sedimentation rate from 4340 - 590 cal yr BP was 0.88 mm/yr; and the sedimentation rate from 5190 - 4340 cal yr BP was 1.44 mm/yr (Fig. 2).

4.2 Core stratigraphy and geochemical characteristics

Core ROC-4 consists of two different types of sediments (Fig. 2). Silt-clay sediments in brownish color occur from 525 to 40 cm. The core stratigraphy and geochemical profiles show

184 relatively stable signals throughout these brownish silt-clay sediments. The sand, silt, and clay
185 fractions vary slightly from 0-5%, 40-50%, and 50-60 %, respectively, in this section, and the sand
186 and silt fractions increase progressively from 150 to 40 cm. The contents of water (50-60 %),
187 organic matter (5-15 %), and carbonates (2-5 %) and the concentrations of Ca (2000-5000 ppm)
188 and Sr (50-100 ppm) are also consistent throughout this section. Nonetheless, a few sediment
189 layers exhibit some variations. Grain-size data indicate that sediment intervals at 320, 280, and
190 100 cm have higher contents (2-5 %) of sand and silt fractions comparing with other intervals in
191 this section. XRF data also reveal a few layers with elevated Ca and Sr contents; particularly,
192 sediment intervals at 195-215 cm have 10 to 20 times higher concentrations of Ca (20000 to 40000
193 ppm) and slightly higher concentrations of Sr in relative to other intervals. In addition, some
194 charcoal fragments, rootlets, and leaflets were also found throughout this section, but overall, the
195 stratigraphy and geochemical datasets show stable results in this silt-clay section (Fig. 2).

196 Above the silt-clay section is a 40-cm layer of sediments consisting of muddy-sand, shell
197 fragments, foraminifera, and some quartz grains and gravels (Fig. 2). Grain-size analysis shows
198 that the sand (10-15 %) and silt (> 50 %) fractions in this section are higher than the silt-clay
199 section beneath. In particular, the top 10 cm of core ROC consists of mainly shell fragments and
200 foraminifera. Macroscopic analysis identified three genera of shells (*Littoraria*, *Anadara*, and
201 *Mactridae*) and two genera of foraminifera (*Elphidium* and *Ammonia*). *Anadara* and *Mactridae*
202 are marine bivalve mollusks, *Littoraria* belongs to a genus of sea snails, and *Elphidium* and
203 *Ammonia* both inhabit in subtidal environments (Yao et al., 2018). Accordingly, the concentrations
204 of Ca and Sr in this section are significantly higher than the silt-clay section, particularly in the top
205 10 cm of the core. The findings suggest that the surface material of core ROC-4 carries a strong
206 marine signal, likely originating from littoral sources.

207

208 *4.3 Pollen data*

209 A total of 26 pollen and spore taxa were identified from core ROC-4, but only palynomorphs
210 occurring at > 2% in any interval were shown individually in Figure 2. All minor pollen taxa (<
211 2%) were grouped together as "other upland taxa" and "other swamp taxa" in Figure 2. The pollen
212 assemblage in Zone A (525-390 cm; ~5190 - 4240 cal yr BP) is dominated by TCT (Taxodiaceae,
213 Cupressaceae, and Taxaceae), Amaranthaceae, and Poaceae. In particular, the pollen assemblages
214 in most intervals contain 10-20% of TCT, a common swamp taxon, reaching their highest
215 percentages in the core. The percentages of Amaranthaceae (up to 20%), Poaceae (< 20%), *Pinus*
216 (up to 30%), and *Quercus* (up to 20%) are relatively high in most intervals in Zone A. Unlike TCT,
217 these taxa are prolific pollinators that produce enormous amount of pollens (Traverse, 2007).
218 Therefore, based on CONISS (Grimm, 1987) and the relative abundance of TCT, Zone A
219 demonstrates typical palynological features of a swamp environment in Louisiana (Ryu et al.,
220 2018). In addition, the concentrations of charcoal fragments and total pollen sum are at 20000-
221 60000 and 5000-17000 counts/cm^3, respectively (Fig. 2).

222 Zone B (390-320 cm; ~4240 to 3440 cal yr BP) is dominated by forest taxa. The percentages
223 of *Pinus* and *Quercus* are up to 60% and 25% in this zone, both reaching their highest percentages
224 in the core. On the contrary, the percentages of other major taxa that are common in the Zone A
225 (TCT, Amaranthaceae, and Poaceae) all decrease in Zone B. The concentrations of charcoal
226 fragments and total pollen sum are at 30000-40000 and 9000-16000 counts/cm^3, respectively (Fig.
227 2). Zone B demonstrates palynological features of a maritime forest environment.

228 The pollen assemblage in Zone C (320 to 160 cm; ~3340 to 1520 cal yr BP) is characterized
229 by an increase in TCT pollen and a decrease in *Pinus* pollen, a change back to swamp environment

from maritime forest environment. Notably, a few grains (< 1%) of *Avicennia* (black mangrove) pollen and a small number of foraminifera linings are also found in Zone C. The concentrations of charcoal fragments and total pollen sum are at 20000-50000 and 12000-15000 counts/cm^3, respectively (Fig. 2).

The pollen assemblage in Zone D (160 to 40 cm; ~1520 to 300 cal yr BP) is characterized by a significant increase in marsh taxa and a 10-fold increase in charcoal fragments (up to 1,800,000 counts/cm^3). The percentages of Amaranthaceae (up to 40%) and Poaceae (up to 25%) reach their highest in the core, while pollen percentages of TCT, *Pinus*, and *Quercus* decease. Particularly, *Batis maritima* starts to appear in the pollen assemblage in this zone and increase towards the top. The pollen of *Sagittaria*, a common marsh plant, begin to appear in Zone D. The pollen assemblage in Zone D exhibits typical palynological features of a coastal marsh environment.

Zone E (40 to 0 cm; 300 cal yr BP to present) is characterized by the dominance of *Batis maritima* (saltwort) pollen. This taxon accounts for 30% of the total pollen sum at the bottom of the zone, increasing toward the top of the core where it reaches over 80% of the total pollen sum. Accordingly, the pollen concentration also significantly increases in Zone E because *Batis maritima* is a very prolific pollen producer (Traverse, 2007). Meanwhile, all the other pollen taxa decrease in most intervals. Noticeably, significant increase in foraminifera linings also occurs in this zone. These palynological features resemble a typical beach and saltmarsh environment in southwest Louisiana (Yao et al., 2018).

4.4 Numerical Analysis of pollen data

Percentage data of 12 major pollen taxa (defined as those occurring at and > 5% in most intervals) were used in a PCA. On the PCA biplot showing the distribution of pollen assemblages

and 12 major pollen taxa (Fig. 3), the first two principal components (PC) account for 29.83% and 21.41% of the variance, respectively (Table S1-S4). Along PC1 axis, *Batis maritima*, a succulent plant thriving in saline environment, have the highest positive loading, whereas bottomland hardwood forest species (*Pinus*, *Liquidambar*, and *Quercus*) have the highest negative loadings. It is likely that PC1 represents a salinity gradient whereby salinity increases from negative toward the positive end of the axis. On PC2, trees and succulent plants (*Pinus*, *Liquidambar*, and *Batis maritima*) have the highest positive loadings. All three taxa, especially *Batis maritima*, adapt to dry or upland environment (Traverse, 2007). At the other end of the axis, wetland and aquatic plants (Poaceae, Cyperaceae, Asteraceae, and *Sagittaria*) have the highest negative loadings. All these taxa, especially *Sagittaria*, an emergent macrophyte, can adapt to water-logged or wetland environment (Traverse, 2007). Thus, it is reasonable to infer that PC2 denotes a hydrological gradient reflecting the moisture content. Accordingly, the PCA biplot is divided into 4 quadrants representing 4 sub-environments, in a clockwise direction, which are Beach (dry and saline), Marsh (wet and saline), Swamp (wet and fresh), and Maritime forest (dry and fresh) environment.

Figure 3A shows the distribution of all pollen assemblages on the PCA biplot, and Figure 3B shows the total pollen sum of each ecological group following the inferred pollen zonation discussed in Figure 2. From the bottom to the top of the core, numerical analysis of pollen data shows that all samples in Zone A fall into the Swamp quadrant (bottom left); all samples in Zone B are located in the Maritime forest quadrant (top left); most samples in Zone C fall back into the Swamp quadrant (bottom left); all samples in Zone D belong to the Marsh quadrant (bottom right); and all samples in Zone E fit exclusively in the Beach quadrant (top right). Hence, the PCA of pollen assemblages is consistent with the inferred pollen zones delineated by CONISS.

5. Discussion

5.1 Holocene coastal morphodynamics and ecosystem development in southwestern Louisiana

Overall, the sedimentary and geochemical datasets show consistent stratigraphic features throughout the core (Fig. 2), suggesting that most intervals within a zone in the sediment profile originated from the same sediment source. Figure 4 illustrates the inferred shoreline and paleoecological history at Rockefeller Wildlife Refuge since the mid-Holocene based on numerical and empirical analyses of pollen data, in relation to the established phases of Mississippi River Delta development (Fig. 4). Between 5190 and 4240 cal yr BP, numerical analysis shows that the pollen assemblage in Zone A is consistent with the pollen signature of a freshwater swamp in Louisiana (Figs. 2 & 3) (Ryu et al., 2018). Such areas are dominated by baldcypress (*Taxodium distichum*), a deciduous conifer most commonly found in freshwater swamps (Lopez, 2003). These ecosystems are typically located in areas 50-100 km inland from the Gulf shorelines (Glick et al., 2013). Thus, our record suggests that the relative sea-level (RSL) was much lower than the present level from 5190 to 4240 cal yr BP, and the shoreline at RWR was likely many kilometers seaward relative to today.

In the meantime, to the east of RWR, the Sale-Cypremont complex (4600-3500 BP), situated at the westernmost position and the closest to our study area among the 6 complexes, was forming during the end of the freshwater swamp stage (Fig. 4). Concurrently, pollen data indicate that the baldcypress swamp in our study area was replaced by *Pinus*, *Quercus*, and *Liquidambar* (Fig. 2), a transition from a longer-hydroperiod freshwater swamp to a dryer maritime forest during 4240-3440 cal yr BP (Fig. 3). Along a typical vegetation zonation pattern across coastal zones in North America, maritime forests occupy areas further inland from freshwater swamps (Traverse, 2007). Hence, shorelines at the RWR was further seaward during the maritime forest stage relative

299 to the freshwater swamp stage (Fig. 4). Such vegetation transition at RWR was consistent with the
300 cyclic delta-building process of the Mississippi River that when the delta lobe switched to a
301 western position, significantly higher suspended sediment load from the Mississippi River would
302 have been transported to the west by the longshore currents - replenishing the coastal zones and
303 resulting in shoreline progradation in southwestern Louisiana (McBride et al., 2007; Owen, 2008;
304 Rosen and Xu, 2011). In particular, the development of maritime forest, which was made possible
305 by shoreline progradation in our study area during 4240-3440 cal yr BP, was synchronous with the
306 timeline of the Sale-Cypremont complex (4600-3500 BP). Thus, all the evidence so far suggests
307 that the Mississippi River Delta Complex is closely associated with the coastal morphodynamics
308 and ecosystem development in southwestern Louisiana.

309 Nevertheless, when the Mississippi River changed its course to the east during the next two
310 delta cycles (Teche and St. Bernard), the Holocene geomorphological history of the southwestern
311 Louisiana coastlines reached a turning point at 3440 cal yr BP when the shoreline dynamics
312 changed from progradational to retrogradational (Fig. 4). This transition is clearly recorded by the
313 proxy record (Figs. 2 & 3). Baldcypress pollen started to rise again in Zone C (3440-1520 cal yr
314 BP), while the maritime forest taxa started to decrease. Although marine influence was still
315 negligible during this period, this vegetation transition was in contrast to Zones A & B. The
316 transition from maritime forest back to baldcypress swamp suggests a gradual rising of the water
317 table, hence, clear evidence of shoreline retreat in our study area.

318 The pollen evidence suggests that shoreline retreat continued throughout Zone D (1520-
319 300 cal yr BP). With the delta lobe remaining at an eastern position during the Lafourche (1000-
320 300 BP) and Plaquemine-Balize (750 BP to present) phases (Fig. 4), the freshwater swamp taxa at
321 RWR were progressively replaced by marsh taxa (Fig. 3). Furthermore, foraminifera linings, an

indicator of marine environment, started to appear with greater regularity during this period. Sand fraction also started to increase in Zone D, indicating a more dynamic environment with higher wave energy (Xu et al., 2016, 2011). In addition, the halophyte *Batis maritima* started to appear while baldcypress declined (Fig. 2). Historically, cypress swamp degradation in Louisiana is attributed to erosion and saltwater intrusion (Roberts, 1997; Glick et al., 2013; Liu et al., 2015;Ryu et al., 2018). These evidences suggest that our study area was turning into a coastal marsh environment with more marine influence. Today, similar coastal marsh occurs as an ecotone between freshwater swamp and beach ridge in RWR (Selman et al., 2011; Yao et al., 2018). Using it as a modern analog, it could be inferred that between 1500 and 300 cal yr BP, freshwater environment at RWR was transforming into brackish marsh environment as marine retrogradation continued.

Finally, since ~400 yr BP, while the main distributary basin of the Mississippi River - Plaquemine-Balize complex remained active, a second distributary basin - the Atchafalaya-Wax Lake complex formed in southwestern Louisiana (Fig. 4). Based on 31 years (1980–2010) of total suspended sediment inflow/outflow data, the Atchafalaya River was delivering ~33 megaton (10^6 tons) of total suspended sediments (TSS) to the Gulf every year (Rosen and Xu, 2015), resulting in a net land gain of 59 km^2 (1989-2010) in the basin (Rosen and Xu, 2013). However, situated at ~100 km to the west of Atchafalaya River mouth, the shoreline at RWR was not replenished by such enormous sediment input (Fig. 5). The pollen data show that *Batis maritima* kept increasing from 300 cal yr BP and became the dominant taxon in Zone E. Meanwhile, other marine indicators including sand fraction (Xu et al., 2016), % carbonate (Yao and Liu, 2017), concentration of Ca and Sr (Yao and Liu, 2018; Yao et al., 2019), and foraminifera linings (Yao et al., 2018) all increased significantly in Zone E. This multi-proxy signature highly resembles the shelly beach

345 environment occurring at the interface between coastal marshes and the Gulf at RWR today
346 (Selman et al., 2011; Yao et al., 2018). The pollen concentration also increased significantly at
347 ~300 cal yr BP, coincident with the increase in *Batis maritima*, a prolific pollen producer.
348 Therefore, the modern beach environment replaced the marsh environment at RWR since 300 cal
349 yr BP due to shoreline retrogression, even though two new sub-deltas (the Atchafalaya and the
350 Wax Lake deltas) formed to the east of our study area (Fig. 4). Overall, when the Mississippi River
351 Delta was at its westerly position as during the Sale-Cypremont phase 4600-3500 years ago, the
352 shoreline at RWR was prograding and our coring site was situated farther inland from the coast.
353 Conversely, when the Mississippi River Delta lobe switched to more easterly positions during the
354 subsequent Teche, St. Bernard, Lafourche, and Plaquemine-Balize phases, shoreline retrogression
355 at RWR started at ~3340 cal yr BP and continued to the present day. Thus, shoreline fluctuations
356 at RWR were tied to the Mississippi River Delta Switch (Fig. 4). Table S5 in the supplementary
357 content synthesize the multi-proxy dataset and further elaborates the correspondences among
358 different systems.
359
360 *5.2 Evidence of possible paleohurricane events*
361 Several sediment intervals in the core show signs of possible disturbance events. Higher
362 sand and silt fractions were found at 320, 280, 100, and 50 cm, and elevated Ca and Sr
363 concentrations occur at 280, 200, 140, and 20-0 cm. Higher contents of sand (Williams, 2009), Ca,
364 and Sr have been described as indicators of prehistorical hurricane events (Woodruff et al., 2009;
365 Yao et al., 2018; McCloskey et al., 2018). While any one of these lines of evidences may not be
366 conclusive indicators of paleohurricane events *per se*, it is notable that at least two of the
367 stratigraphic levels, at 280 cm and 200 cm, are marked by elevated concentrations of Ca and Sr,

368 and/or higher sand and silt fractions. It is also interesting that these levels containing these
369 characteristics occur during the time interval between ~3000 and 900 years BP, generally
370 corresponding to the "hyperactive period" (~3800-1000 al yr BP) in paleohurricane activity
371 documented in the Gulf of Mexico (Liu and Fearn, 2000) and the Caribbean basin (Giry et al.
372 2012; Aragón-Moreno et al. 2018). It is therefore possible that increased hurricane activities in the
373 Gulf of Mexico directly or indirectly affected southwestern Louisiana during the hyperactive
374 period.

375 The biggest of these possible hurricane events, marked by prominent peaks in both Ca and
376 Sr, occurred at 200 cm (~2000 cal yr BP) near the top of Zone C, at a time when the coring site
377 was transitioning from a swamp to a marsh as the shoreline was retreating, making the site more
378 vulnerable to storm surge from extreme hurricanes than before. Another possible event layer,
379 occurring at 100 cm (~900 cal yr BP) in the upper part of Zone D, is marked by a greater fraction
380 of sand. While this could be deposited by storm surge or overwash processes during a
381 paleohurricane event, this explanation cannot be firmly established as it is not supported by any
382 corroborating evidence from the marine incursion proxies such as Ca and Sr. Alternatively, other
383 disturbance mechanisms, such as fluvial flooding from extreme precipitation events, could be
384 responsible for the deposition of sand layers in coastal wetland sediments (Wang et al., 2019).
385 However, no large rivers are present near our study site today.

386 The uppermost 20 cm of the sediment core from Louisiana's Chenier Plain is marked by
387 prominent peaks in carbonates, Ca and Sr concentrations, and the abundance of foraminifera tests
388 and shells. In a geochemical study of the nearby Calcasieu River estuary, He and Xu (2016) found
389 a strong increasing trend of these two elements from upstream to the river mouth. These findings
390 strongly suggest marine incursion and/or overwash events caused by hurricane activity. Multi-

391 proxy data from three sediment monoliths collected within 50 m from the coring site contained
392 two storm deposits attributed to two recent hurricanes—Hurricane Ike (2008) and Hurricane Rita
393 (2005)—in the top 20 cm (Yao et al., 2018). These two storm deposits are similarly represented in
394 the upper 20 cm of core ROC-4. An analysis of remote sensing images from 1998 to 2017 showed
395 that the shoreline at RWR retreated by 276 m over this 20-year period, at a rate of 14.5 m/year—
396 the highest rate of coastal recession in the entire Gulf of Mexico (Yao et al., 2018; Dietz et al.,
397 2018) (Fig. 5). During the last 300 years (Zone E) rapid shoreline retreat has rendered the coring
398 site into a backbarrier setting behind a shelly beach and berm, thereby becoming increasingly
399 subject to the impacts of storm surge and overwash processes. Thus, the impacts of these two
400 recent hurricanes are prominently recorded in the stratigraphy of core ROC-4.
401
402 *5.3 Implications for coastal morphodynamics and sustainability in southwestern Louisiana*
403 The multi-proxy record in this study has demonstrated that coastal morphodynamics in
404 southwestern Louisiana was closely tied to the position of the Mississippi River Delta complexes
405 (Fig. 4). During the mid-Holocene when the main Mississippi River Delta was situated in the west
406 (i.e., the Sale-Cypremont complex), sedimentation rate at RWR was 1.44 mm/yr—roughly equal
407 to the rate of RSL rise (1.5 mm/ yr) at that time (Törnqvist et al., 2004)—the shoreline at RWR
408 was prograding due likely to sufficient sediment supplies by the Mississippi-Atchafalaya River
409 system. Subsequently, when the delta switched to more easterly positions (Teche, St. Bernard,
410 Lafourche, and Plaquemine-Balize complexes) after 3500 yr BP, sedimentation rate at RWR
411 decreased to 0.88 mm/yr, a decrease of almost 40% and slower than the rate of regional sea-level
412 rise (~1 mm/yr) (Donoghue, 2011), causing the shoreline at RWR to retreat rapidly. During the
413 past 300 years when the Atchafalaya-Wax Lake complex developed in areas closer to southwest

414 Louisiana, sedimentation rate at RWR increased to 1.19 mm/yr. However, the modern rate of RSL
415 rise in Louisiana also increased to almost twice as high (2 mm/yr) (Penland and Ramsey, 1990;
416 Donoghue, 2011), thereby resulting in accelerated coastal retrogression. The shoreline at RWR
417 was retreating at an alarming rate of 14.5 m/yr since the 1990s (Fig. 5), and this rate was even
418 higher during years with hurricane strikes (Yao et al., 2018). These numbers exhibit a strong
419 relationship between shoreline fluctuations and the rate of sedimentation versus the rate of RSL
420 rise. When the sedimentation rate exceeds the rate of RSL, the shoreline at RWR is sustained.
421 Conversely, when the sedimentation rate falls lower than the rate of RSL rise, the shoreline at
422 RWR retreats, resulting in significant land loss in southwestern Louisiana. The driving force
423 behind the variations in sedimentation rate at RWR is the position of the Mississippi River Delta,
424 which is the main source of sediment supply for the coastal plain of southwestern Louisiana.

425 At present, the Atchafalaya River is the main source of sediment supply for the
426 southwestern Louisiana coastlines (Xu, 2010; Rosen and Xu, 2011). The Atchafalaya-Wax Lake
427 complex annually delivers ~30% of Mississippi River's water and 33 megatons of total suspended
428 sediments (TSS) into the Gulf of Mexico (Rosen and Xu, 2015). However, this amount of annual
429 sediment supply is insufficient to counter the rate of RSL rise and to replenish the coastal wetlands
430 at RWR. This condition is reflected in the delicate location where RWR is situated at today with
431 regard to Louisiana's coastal morphodynamics, whereby the shorelines to the east are rapidly
432 prograding due to sufficient sediment supply from the Atchafalaya River (Xu, 2010; Rosen and
433 Xu, 2013) but the Chenier Plain to the west is rapidly eroding as the distance from the Atchafalaya
434 River mouth increases (Roberts, 1997; McBride et al., 2007; Owen, 2008; Rosen and Xu, 2011).
435 Although the TSS input from the Plaquemine-Balize delta complex, the main delta of the modern
436 Mississippi River, is much higher, this sediment source is over 300 km to the east of RWR – too

far and too negligible to replenish the wetlands on the southwestern Louisiana coastlines (Xu, 2010; Wang and Xu, 2018). The four minor rivers in southwestern Louisiana - Sabine, Calcasieu, Mermentau, and Vermilion Rivers (Fig. 1), totally carried 6.86 x 10^6 tons of sediments over a 20-year period from 1990-2010, but most of this sediment was unable to reach the coastline, and the portion that did reach the coastline was transported to Texas by the long-shore currents (Rosen and Xu, 2011). Therefore, increasing the sediment supply from the Atchafalaya River to the east is the only viable option to combat shoreline retreat and coastal land loss in RWR and southwestern Louisiana.

One possible solution for replenishing the coastal wetlands at RWR will be to divert more sediments from the main Mississippi River—now carrying about 75% of the annual discharge—to the Atchafalaya River via the Old River Control Structure near Red River Landing, Louisiana (Rosen and Xu, 2013; 2015). However, this will further reduce the sediment supply to the already sinking southeastern Louisiana coasts, especially around the bird-foot delta (Wang and Xu, 2018). In fact, the State of Louisiana has proposed in its 2017 Coastal Master Plan (CPRA, 2017) that sediment diversions from the lower Atchafalaya to the east Terrebonne Parish be implemented, which could further reduce riverine sediment supply to the Chenier Plain. All the four nearby rivers flowing through Louisiana's Chenier Plain deliver only a marginal quantity of sediment (in total: 3.43 x 10^5 tons per year) to the chenier coast, and the sediment load has been declining (Rosen and Xu, 2011). Therefore, the restoration of coastal Louisiana is facing a dilemma of either saving one side of the coast or losing both sides.

6. Conclusions

This study utilizes a multi-proxy approach to reconstruct the sedimentary and ecological

history of the Chenier Plain in southwestern Louisiana, one of the world's largest chenier plains, which is located west of the Mississippi-Atchafalaya River system. The findings from this study suggest a strong influence of the river on the development of the Chenier Plain and its ecosystems in the past 5,200 years. Since the mid-Holocene, the shoreline of the Chenier Plain fluctuated between progradation and retrogradation, and this fluctuation was closely tied to the Mississippi River Delta Switch. The pollen record shows that coastal ecosystems at the eastern end of Louisiana's Chenier Plain changed from swamp to maritime forest during 5200-3440 cal yr BP, and from swamp to marsh and then to beach/dune community after 3440 cal yr BP. Shoreline retrogradation at the study site began around ~3440 cal yr BP and persisted to the present day. In particular, the shoreline at the Rockefeller Wildlife Refuge was retreating at an alarming rate of 14.5 m/yr since the 1990s. The shoreline fluctuation and the rate of sedimentation are also associated with the rate of relative sea level rise. When the sedimentation rate falls below the relative sea level rise rate, the shoreline of the Chenier Plain retrogrades,
resulting in significant land loss in southwestern Louisiana. Based on these findings, we conclude that Louisiana's Chenier Plain will continue to retreat because of the continuous sea level rise and reduction of riverine sediment supply.

Acknowledgements

This research was supported by grants from the U.S. National Science Foundation (Grants #1759715, 1212112), NOAA/Louisiana Sea Grant, Louisiana Coastal Protection and Restoration Authority (CPRA Coastal Science Scholarship funds), and the Ministry of Science and Technology of the People's Republic of China (Grant #2017YFE0107400). During the preparation of the manuscript, Y. Jun Xu received funding support from a US Department of Agriculture Hatch Fund

project (project number: LAB94230). The statements, findings, and conclusions are those of the authors and do not necessarily reflect the views of the funding agencies. We thank Terrence McCloskey, Thomas Bianchette, and Joanna Plattsmier for their assistance in fieldwork. Special thanks go to Phillip "Scooter" Trosclair and other staff members from the Rockefeller Wildlife Refuge for field and logistical support during this study.

Data Availability

All of the datasets produced in this article will be stored at the Neotoma Paleoecology Database (https://www.neotomadb.org) upon publication and accessible to the public for free.

Figure Captions

Figure 1. Location of the sediment core ROC-4 (red star) at the eastern end of the Chenier Plain in southwestern Louisiana, USA. Sediment supply in the area is strongly influenced by the Mississippi River, which changed its course several times in the past 5,000 years (in chronological order based on Roberts, 1997; Day et al., 2007; and McBride et al., 2007).

Figure 2. The age-depth model, litholog, grain-size, LOI, XRF, and pollen results of core ROC-4 from southwestern Louisiana.

Figure 3. (A) PCA biplot showing the distribution of 12 main pollen taxa and pollen assemblages collected from core ROC-4, plotted along components 1 and 2. (B) Vegetation sub-environments on the chenier plain based on CONISS and PCA biplot.

Figure 4. (Left) Conceptual diagram illustrating the Holocene coastal morphodynamics and ecosystem development on Louisiana's Chenier Plain at the Rockefeller Wildlife Refuge; (Right) corresponding developmental phases of the Mississippi River Delta Switch.

Figure 5. Remote sensing images showing rapid shoreline retrogradation on Louisiana's Chenier Plain at the Rockefeller Wildlife Refuge from 1998 to 2017. The red lines perpendicular to the shoreline show the distance between the core ROC-4 location and the seaward edge of the beach (the white area on satellite image) on every satellite image. These lines were used as references to measure the site-to-sea distance for when the satellite image was taken. The figure is a modified version from that in Yao et al. (2018).

517 **Table Caption**

518 **Table 1**. Radiocarbon dating results for core ROC-4 from southwestern Louisiana.

519

520

521 **References**

522 Aragón-Moreno, A.A., Islebe, G.A., Roy, P.D., Torrescano-Valle, N., Mueller, A.D., 2018.
523 Climate forcings on vegetation of the southeastern Yucatán Peninsula (Mexico) during the
524 middle to late Holocene. Palaeogeogr. Palaeoclimatol. Palaeoecol. 495, 214–226.

525 Blum, M.D., Roberts, H.H., 2009. Drowning of the Mississippi Delta due to insufficient sediment
526 supply and global sea-level rise. Nat. Geosci. 2, 488–491.

527 Bush, N., Bush, E., Sokolova, Y., Bush, N., Blanchard, P., 2018. Utilizing the physiological
528 adaptation mechanisms of coastal plants for vegetative restoration of barrier islands. Ocean
529 Coast. Manag. 161, 222–227.

530 Chmura, G.L., Stone, P.A., Ross, M.S., 2006. Non-pollen microfossils in Everglades sediments.
531 Rev. Palaeobot. Palynol. 141, 103–119.

532 Coleman, J.M., 1988. Dynamic changes and processes in the Mississippi River delta. GSA Bulletin
533 100, 999–1015.

534 Coleman, J.M., Roberts, H.H., Gregory W. Stone, 1998. Mississippi River Delta: An Overview. J.
535 Coast. Res. 14, 699–716.

536 Couvillion, B.R., Barras, J.A., Steyer, G.D., Sleavin, W., Fischer, M., Beck, H., Trahan, N.,
537 Griffin, B., Heckman, D., 2011. Land area change in coastal Louisiana from 1932 to 2010.

538 Couvillion, B.R., Beck, H., 2013. Marsh Collapse Thresholds for Coastal Louisiana Estimated
539 Using Elevation and Vegetation Index Data. J. Coast. Res. 63, 58–67.

540 Couvillion, B.R., Beck, H., Schoolmaster, D. and Fischer, M., 2017. Land area change in coastal
541 Louisiana (1932 to 2016) (No. 3381). US Geological Survey.

542 CPRA, 2007. Coastal Protection and Restoration Authority, 2017 Coastal Master Plan
543 http://coastal.la.gov/our-plan/2017-coastal-master-plan/ (accessed February 2020).

544 CPRA, 2020. Coastal Protection and Restoration Authority [WWW Document]. Louisiana Coastal

545 Protection and Restoration Authority. URL http://coastal.la.gov/ (accessed 1.20).
546 Day, J.W., Jr, Boesch, D.F., Clairain, E.J., Kemp, G.P., Laska, S.B., Mitsch, W.J., Orth, K.,
547 Mashriqui, H., Reed, D.J., Shabman, L., Simenstad, C.A., Streever, B.J., Twilley, R.R.,
548 Watson, C.C., Wells, J.T., Whigham, D.F., 2007. Restoration of the Mississippi Delta: lessons
549 from Hurricanes Katrina and Rita. Science 315, 1679–1684.
550 Dean, W.E., 1974. Determination of carbonate and organic matter in calcareous sediments and
551 sedimentary rocks by loss on ignition; comparison with other methods. J. Sediment. Res. 44,
552 242–248.
553 Delcourt, P.A., Delcourt, H.R., 1996. Quaternary paleoecology of the Lower Mississippi Valley.
554 Eng. Geol. 45, 219–242.
555 Delcourt, P.A., Delcourt, H.R., Brister, R.C., Lackey, L.E., 1980. Quaternary Vegetation History
556 of the Mississippi Embayment 1 , 2. Quat. Res. 13, 111–132.
557 Dietz, M., Liu, K.-B., Bianchette, T., 2018. Hurricanes as a Major Driver of Coastal Erosion in the
558 Mississippi River Delta: A Multi-Decadal Analysis of Shoreline Retreat Rates at Bay
559 Champagne, Louisiana (USA). Water 10, 1480.
560 Donnelly, J.P., Webb, T., III, Murnane, R., Liu, K.-B., 2004. Backbarrier sedimentary records of
561 intense hurricane landfalls in the northeastern United States. Hurricanes and Typhoons: Past,
562 Present, and Future 55, 58–95.
563 Donoghue, J.F., 2011. Sea level history of the northern Gulf of Mexico coast and sea level rise
564 scenarios for the near future. Clim. Change 107, 17.
565 Elsner, J.B., Jagger, T.H., Liu, K.-B., 2008. Comparison of Hurricane Return Levels Using
566 Historical and Geological Records. J. Appl. Meteorol. Climatol. 47, 368–374.
567 Frazier, D.E., 1967. Recent deltaic deposits of the Mississippi River: their development and

568 chronology. Gulf Coast Association of Geological Societies, Transactions 17, 287–316.
569 Givens, C.R., Givens, F.M., 1987. Age and Significance of Fossil White Spruce (Picea glauca),
570 Tunica Hills, Louisiana-Mississippi. Quat. Res. 27, 283–296.
571 Giry, C., Felis, T., Kölling, M., Scholz, D., Wei, W., Lohmann, G. and Scheffers, S., 2012. Mid-
572 to late Holocene changes in tropical Atlantic temperature seasonality and interannual to
573 multidecadal variability documented in southern Caribbean corals. Earth and Planetary Science
574 Letters, 331, pp.187-200.
575 Glick, P., Clough, J., Polaczyk, A., Couvillion, B., Nunley, B., 2013. Potential Effects of Sea-
576 Level Rise on Coastal Wetlands in Southeastern Louisiana. J. Coast. Res. 63, 211–233.
577 Grimm EC, 1987. CONISS: a Fortran 77 program for stratigraphically constrained cluster analysis
578 by the method of incremental sum of squares. Computers & Geosciences 13(1): 13-35, DOI
579 10.1016/0098-3004(87)90022-7.
580 He, S. and Y.J. Xu. 2016. Spatiotemporal Distributions of Sr and Ba along an Estuarine River with
581 a Large Salinity Gradient to the Gulf of Mexico. Water doi: 10.3390/w8080323.
582 Huntley, B. and Webb III, T. eds., 2012. Vegetation history (Vol. 7). Springer Science & Business
583 Media.
584 Jones, M.C., Wingard, G.L., Stackhouse, B., Keller, K., Willard, D., Marot, M., Landacre, B., E
585 Bernhardt, C., 2019. Rapid inundation of southern Florida coastline despite low relative sea-
586 level rise rates during the late-Holocene. Nat. Commun. 10, 3231.
587 Kemp, G.P., Day, J.W., Yáñez-Arancibia, A., Peyronnin, N.S., 2016. Can Continental Shelf River
588 Plumes in the Northern and Southern Gulf of Mexico Promote Ecological Resilience in a Time
589 of Climate Change? Water 8, 83.
590 Kiage, L.M., 2020. A 1200-year history of environmental changes in Bay Jimmy area, coastal

591 Louisiana, USA. Holocene 30, 201–209.
592 Kiage, L.M., Liu, K.-B., 2009. Palynological evidence of climate change and land degradation in
593 the Lake Baringo area, Kenya, East Africa, since AD 1650. Palaeogeogr. Palaeoclimatol.
594 Palaeoecol. 279, 60–72.
595 King, J.E., Allen, W.H., 1977. A Holocene Vegetation Record from the Mississippi River Valley,
596 Southeastern Missouri. Quat. Res. 8, 307–323.
597 Kolb, C.R., Van Lopik, J.R., 1958. Geology of the Mississippi River deltaic plain, southeastern
598 Louisiana: US Army Corps of Engineers, Waterways Experiment Station. Technical Report 2.
599 Kulp, M., Penland, S., Williams, S.J., Jenkins, C., Flocks, J., Kindinger, J., 2005. Geologic
600 Framework, Evolution, and Sediment Resources for Restoration of the Louisiana Coastal Zone.
601 J. Coast. Res. 56–71.
602 Lam, N.S.-N., Xu, Y.J., Liu, K.-B., Dismukes, D.E., Reams, M., Pace, R.K., Qiang, Y., Narra, S.,
603 Li, K., Bianchette, T.A., Cai, H., Zou, L., Mihunov, V., 2018a. Understanding the Mississippi
604 River Delta as a Coupled Natural-Human System: Research Methods, Challenges, and
605 Prospects. Water 10, 1054.
606 Lam, N.S.-N., Cheng W., Zou L., Cai H., 2018b. Effects of landscape fragmentation on land loss.
607 Remote Sensing of Environment 209:253-262.
608 Liu, K.-B. and Fearn, M.L., 2000. "Reconstruction of prehistoric landfall frequencies of
609 catastrophic hurricanes in northwestern Florida from lake sediment records", Quaternary
610 Research 54: 238-245.
611 Liu, K.-B., 2004. Paleotempestology: Principles, methods and examples from Gulf coast lake
612 sediments, in: Murnane, R.J., Kam-biu, L. (Eds.), Hurricanes and Typhoons: Past, Present and
613 Future. New York: Columbia University Press.

614 Liu, K.-B., Lam, N.S.-N., 1985. Paleovegetational Reconstruction Based on Modern and Fossil
615 Pollen Data: An Application of Discriminant Analysis. Ann. Assoc. Am. Geogr. 75, 115–130.
616 Liu, K.-B., Li, C., Bianchette, T.A., McCloskey, T.A., Yao, Q., Weeks, E., 2011. Storm deposition
617 in a coastal backbarrier lake in Louisiana caused by Hurricanes Gustav and Ike. J. Coast. Res.
618 1866–1870.
619 Liu, K.-B., McCloskey, T.A., Ortego, S., Maiti, K., 2014. Sedimentary signature of Hurricane
620 Isaac in a Taxodium swamp on the western margin of Lake Pontchartrain, Louisiana, USA.
621 Proceedings of the International Association of Hydrological Sciences 367, 421–428.
622 Lopez, J.A., 2003. Chronology and analysis of environmental impacts within the Pontchartrain
623 basin of the Mississippi Delta Plain: 1718-2002. University of New Orleans.
624 McAndrews, J.H., Berti, A.A., Norris, G., 1973. Key to the quaternary pollen and spores of the
625 Great Lakes region. Royal Ontario Museum.
626 McBride, R.A., Taylor, M.J., Byrnes, M.R., 2007. Coastal morphodynamics and Chenier-Plain
627 evolution in southwestern Louisiana, USA: A geomorphic model. Geomorphology 88, 367–
628 422.
629 McFarlan, E., Jr, 1961. Radiocarbon dating of late Quaternary deposits, south Louisiana. Geol.
630 Soc. Am. Bull. 72, 129–158.
631 McIntire, W.G., 1954. Correlation of prehistoric settlements and delta development. Louisiana
632 State University.
633 Michot, T.C., Day, R.H., Wells, C.J., 2010. Increase in black mangrove abundance in coastal
634 Louisiana. Louisiana Natural Resources News.
635 Owen, D.E., 2008. Geology of the Chenier Plain of Cameron Parish, southwestern Louisiana.
636 Geological Society of America Field Guide 14, 27–38.

637 Osland, M.J., et al., 2013. Winter climate change and coastal wetland foundation species: salt
638 marshes vs. mangrove forests in the southeastern United States. Global Change
639 Biology 19(5): 1482-1494.
640 Penland, S., Ramsey, K.E., 1990. Relative Sea-Level Rise in Louisiana and the Gulf of Mexico:
641 1908-1988. J. Coast. Res. 6, 323–342.
642 Reed, D.J., Wilson, L., 2004. Coast 2050: A New Approach to Restoration of Louisiana Coastal
643 Wetlands. Phys. Geogr. 25, 4–21.
644 Roberts, H.H., 1997. Dynamic Changes of the Holocene Mississippi River Delta Plain: The Delta
645 Cycle. J. Coast. Res. 13, 605–627.
646 Rosen, T., Xu, Y.J., 2015. Estimation of sedimentation rates in the distributary basin of the
647 Mississippi River, the Atchafalaya River Basin, USA. Hydrology Research 46, 244–257.
648 Rosen, T., Xu, Y.J., 2013. Recent decadal growth of the Atchafalaya River Delta complex: Effects
649 of variable riverine sediment input and vegetation succession. Geomorphology 194, 108–120.
650 Rosen, T., Xu, Y.J., 2011. Riverine sediment inflow to Louisiana Chenier Plain in the Northern
651 Gulf of Mexico. Estuar. Coast. Shelf Sci. 95, 279–288.
652 Ryu, J., Bianchette, T.A., Liu, K.-B., Yao, Q., Maiti, K.D., 2018. Palynological and Geochemical
653 Records of Environmental Changes in a Taxodium Swamp near Lake Pontchartrain in Southern
654 Louisiana (USA) during the Last 150 Years. J. Coast. Res. 85, 381–385.
655 Schoolmaster, D.R., Stagg, C.L., Sharp, L.A., McGinnis, T.E., Wood, B., Piazza, S.C., 2018.
656 Vegetation Cover, Tidal Amplitude and Land Area Predict Short-Term Marsh Vulnerability in
657 Coastal Louisiana. Ecosystems 21, 1335–1347.
658 Selman, W., Salyers, B., Salyers, C., Perry, G., Elsey, R., Hess, T., Zimorski, S., 2011. Rockefeller
659 Wildlife Refuge Management Plan. Grand Chenier: Louisiana Department of Wildlife and

660 Fisheries.
661 Shaffer, G.P., Wood, W.B., Hoeppner, S.S., Perkins, T.E., Zoller, J., Kandalepas, D., 2009.
662 Degradation of baldcypress--water tupelo swamp to marsh and open water in southeastern
663 Louisiana, USA: an irreversible trajectory? J. Coast. Res. 2009, 152–165.
664 Stuiver, M., Reimer, P.J., Reimer, R., 2020. CALIB Radiocarbon Calibration 7.1 [WWW
665 Document]. Calib 7.1. URL http://calib.org/calib/calib.html (accessed 1.31.20).
666 Schwartz, M. (ed.), 2005. Encyclopedia of Coastal Science. Springer Science & Business Media.
667 Törnqvist, T.E., González, J.L., Newsom, L.A., Van der Borg, K., De Jong, A.F.M., Kurnik, C.W.,
668 2004. Deciphering Holocene sea-level history on the US Gulf Coast: A high-resolution record
669 from the Mississippi Delta. Geol. Soc. Am. Bull. 116, 1026–1039.
670 Traverse, A., 2007. Paleopalynology, Topics in Geobiology. Springer.
671 Urrego, L.E., Bernal, G., Polanía, J., 2009. Comparison of pollen distribution patterns in surface
672 sediments of a Colombian Caribbean mangrove with geomorphology and vegetation. Rev.
673 Palaeobot. Palynol. 156, 358–375.
674 Van Soelen, E.E., Brooks, G.R., Larson, R.A., Sinninghe Damsté, J.S., Reichart, G.J., 2012. Mid-
675 to late-Holocene coastal environmental changes in southwest Florida, USA. Holocene 22, 929–
676 938.
677 Wallace, D.J., Woodruff, J.D., Anderson, J.B., Donnelly, J.P., 2014. Palaeohurricane
678 reconstructions from sedimentary archives along the Gulf of Mexico, Caribbean Sea and
679 western North Atlantic Ocean margins. Geological Society, London, Special Publications 388,
680 481–501.
681 Wang, B., Xu, Y.J., 2018. Decadal-Scale Riverbed Deformation and Sand Budget of the Last 500
682 km of the Mississippi River: Insights into Natural and River Engineering Effects on a Large

683 Alluvial River. Journal of Geophysical Research: Earth Surface 123, 874–890.
684 Wang, L., Bianchette, T.A. and Liu, K.B., 2019. Diatom evidence of a paleohurricane-induced
685 coastal flooding event in Weeks Bay, Alabama, USA. Journal of Coastal Research, 35(3), 499-
686 508.
687 Whitehead, D.R., 1972. Developmental and Environmental History of the Dismal Swamp. Ecol.
688 Monogr. 42, 301–315.
689 Whitehead, D.R., Sheehan, M.C., 1985. Holocene Vegetational Changes in the Tombigbee River
690 Valley, Eastern Mississippi. Am. Midl. Nat. 113, 122–137.
691 Willard, D.A., Bernhardt, C.E., 2011. Impacts of past climate and sea level change on Everglades
692 wetlands: placing a century of anthropogenic change into a late-Holocene context. Clim.
693 Change 107, 59.
694 Willard, D.A., Bernhardt, C.E., Weimer, L., Cooper, S.R., Gamez, D., Jensen, J., 2004. Atlas of
695 pollen and spores of the Florida Everglades. Palynology 28, 175–227.
696 Willard, D.A., Weimer, L.M., Riegel, W.L., 2001. Pollen assemblages as paleoenvironmental
697 proxies in the Florida Everglades. Rev. Palaeobot. Palynol. 113, 213–235.
698 Williams, K., Pinzon, Z.S., Stumpf, R.P., Raabe, E.A., 1999. Sea-level rise and coastal forests on
699 the Gulf of Mexico. US Geological Survey 1500, 20910.
700 Williams, J.W., Shuman, B.N., Webb III, T., Bartlein, P.J., Leduc, P.L., 2004. Late-Quaternary
701 vegetation dynamics in North America: scaling from Taxa to Biomes. Ecological Monographs
702 74(2):309-334
703 Woodruff, J.D., Donnelly, J.P., and Okusu, A., 2009, Exploring typhoon variability over the mid-
704 to-late Holocene: Evidence of extreme coastal flooding from Kamikoshiki, Japan: Quaternary
705 Science Reviews, v. 28, p. 1774– 1785, doi:10.1016/j.quascirev.2009.02.005.

706 Xu, K., Harris, C.K., Hetland, R.D., Kaihatu, J.M., 2011. Dispersal of Mississippi and Atchafalaya
707 sediment on the Texas–Louisiana shelf: Model estimates for the year 1993. Cont. Shelf Res.
708 31, 1558–1575.
709 Xu, K., Mickey, R.C., Chen, Q., Harris, C.K., Hetland, R.D., Hu, K., Wang, J., 2016. Shelf
710 sediment transport during hurricanes Katrina and Rita. Comput. Geosci. 90, 24–39.
711 Xu, Y.J., 2010. Long-term sediment transport and delivery of the largest distributary of the
712 Mississippi River, the Atchafalaya, USA. Sediment Dynamics for a Changing Future 337, 282–
713 290.
714 Xu, Y.J., Lam, N.S.-N., Liu, K.-B., 2018. Assessing Resilience and Sustainability of the
715 Mississippi River Delta as a Coupled Natural-Human System. Water 10, 1317.
716 Yao, Q., Liu, K.-B., 2018. Changes in Modern Pollen Assemblages and Soil Geochemistry along
717 Coastal Environmental Gradients in the Everglades of South Florida. Frontiers in Ecology and
718 Evolution 5, 178.
719 Yao, Q., Liu, K.-B., 2017. Dynamics of marsh-mangrove ecotone since the mid-Holocene: A
720 palynological study of mangrove encroachment and sea level rise in the Shark River Estuary,
721 Florida. PLoS One 12, e0173670.
722 Yao, Q., Liu, K.-B., Platt, W.J., Rivera-Monroy, V.H., 2015. Palynological reconstruction of
723 environmental changes in coastal wetlands of the Florida Everglades since the mid-Holocene.
724 Quat. Res. 83, 449–458.
725 Yao, Q., Liu, K.-B., Ryu, J., 2018. Multi-proxy Characterization of Hurricanes Rita and Ike Storm
726 Deposits in the Rockefeller Wildlife Refuge, Southwestern Louisiana. Journal of Coastal
727 Research 85, 841–845.
728 Yao, Q., Liu, K.-B., Williams, H., Joshi, S., Bianchette, T.A., Ryu, J., Dietz, M., 2019. Hurricane

729 Harvey Storm Sedimentation in the San Bernard National Wildlife Refuge, Texas: Fluvial
730 Versus Storm Surge Deposition. Estuaries Coasts. https://doi.org/10.1007/s12237-019-00639-
731 6
732 Zhang, Z., Yao, Q., Bianchette, T.A., Liu, K.-B., Wang, G., 2019. A multi-proxy quantitative
733 record of Holocene hydrological regime on the Heixiazi Island (NE China): indications for the
734 evolution of East Asian summer monsoon. Clim. Dyn. 52, 6773–6786.

735

736 **Figure 1**

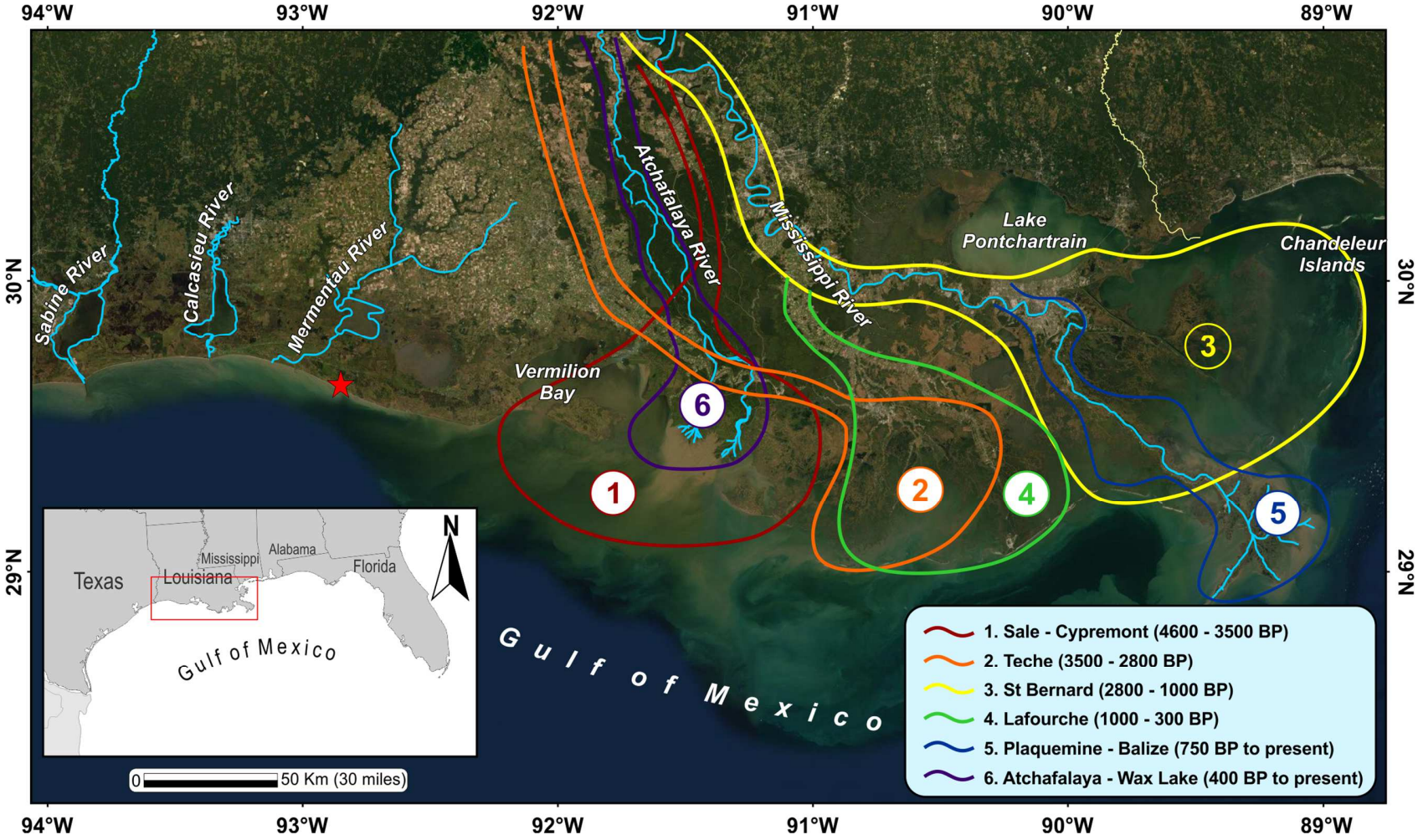

737

738

739 **Figure 2**

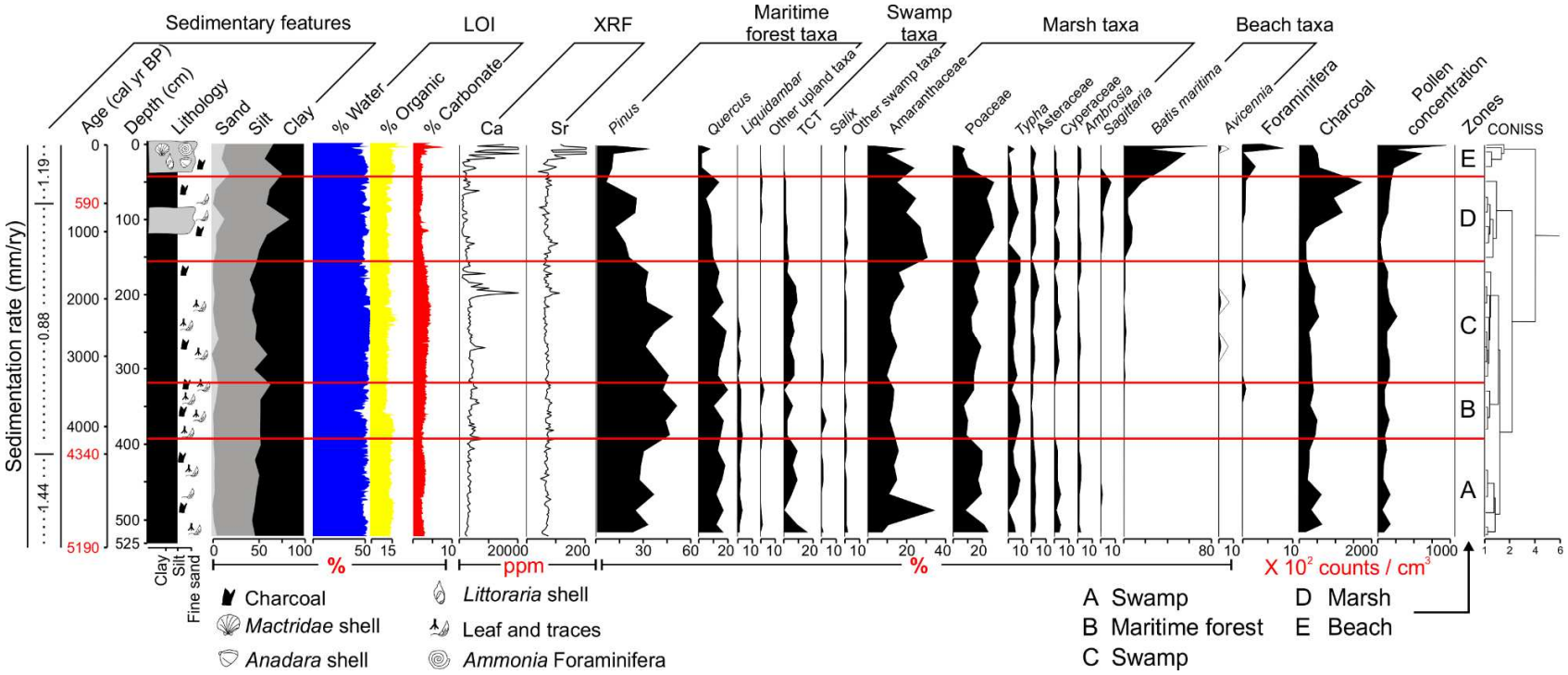

740

741

742 **Figure 3**

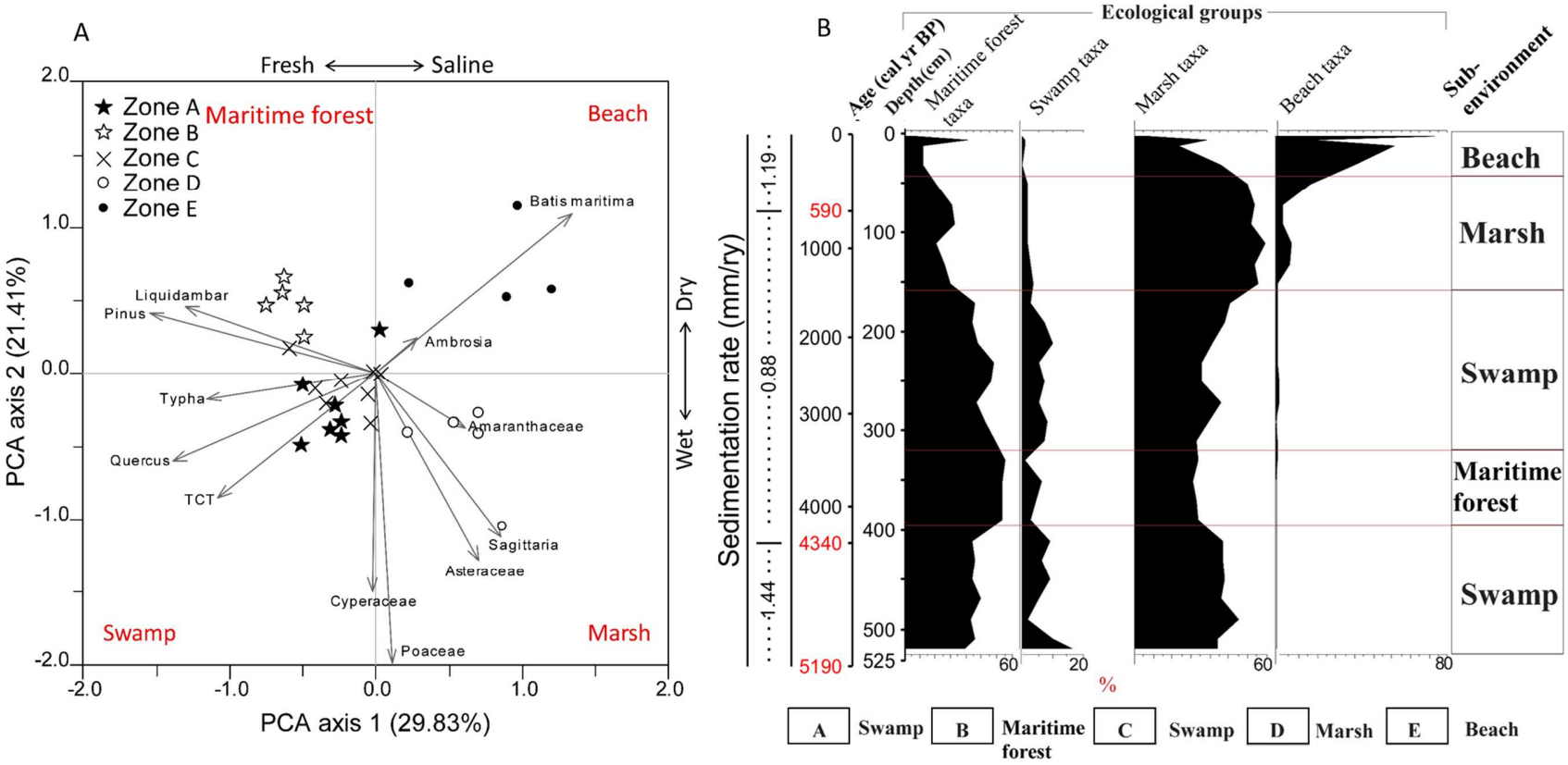

743

744

745

746

747 **Figure 4**

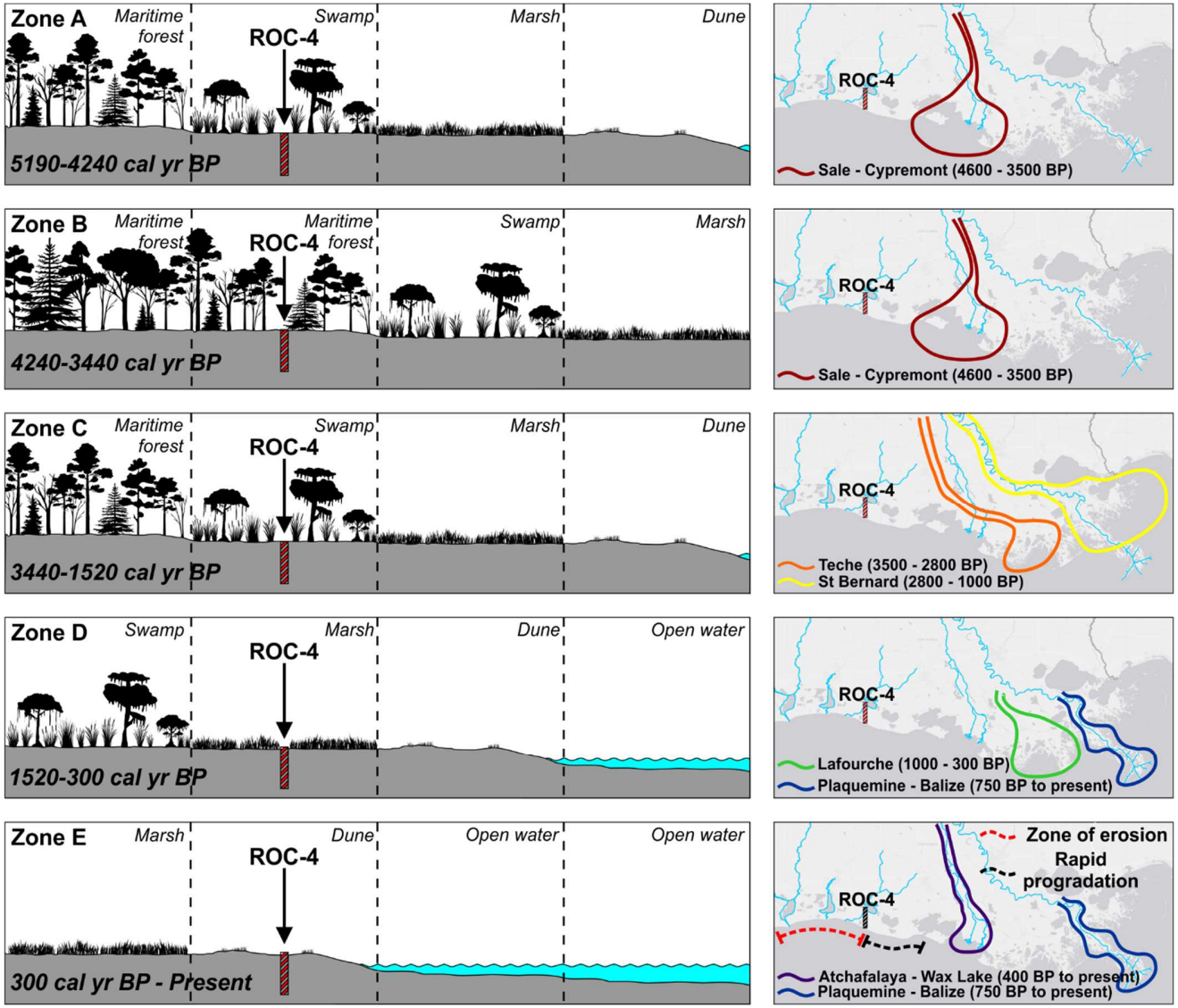

748

749 **Figure 5**

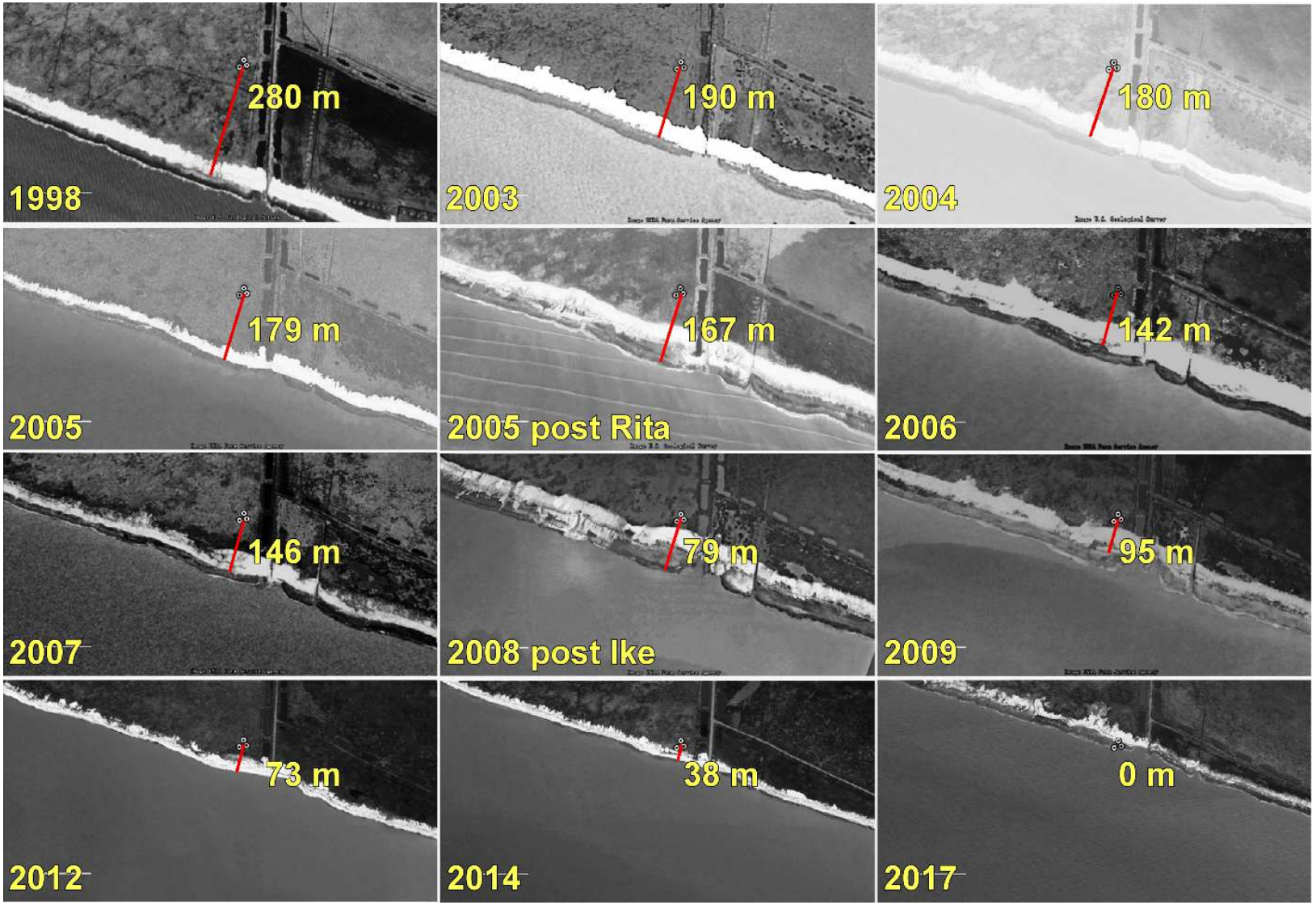

750

751 **Table 1**

Sample depth	Sediment type	Conventional age	Calibrated age (cal yr BP)	2-sigma calibration (cal yr BP)
78 cm	Organic sediment	580 +/- 30 BP	590	533 – 569 (0.333 %)
				582 – 649 (0.667 %)
403 cm	Organic sediment	3900 +/- 30 BP	4340	4247 – 4418 (100 %)
525 cm	Organic sediment	4530 +/- 30 BP	5190	5053 – 5190 (0.663 %)
				5214 – 5309 (0.337 %)

752

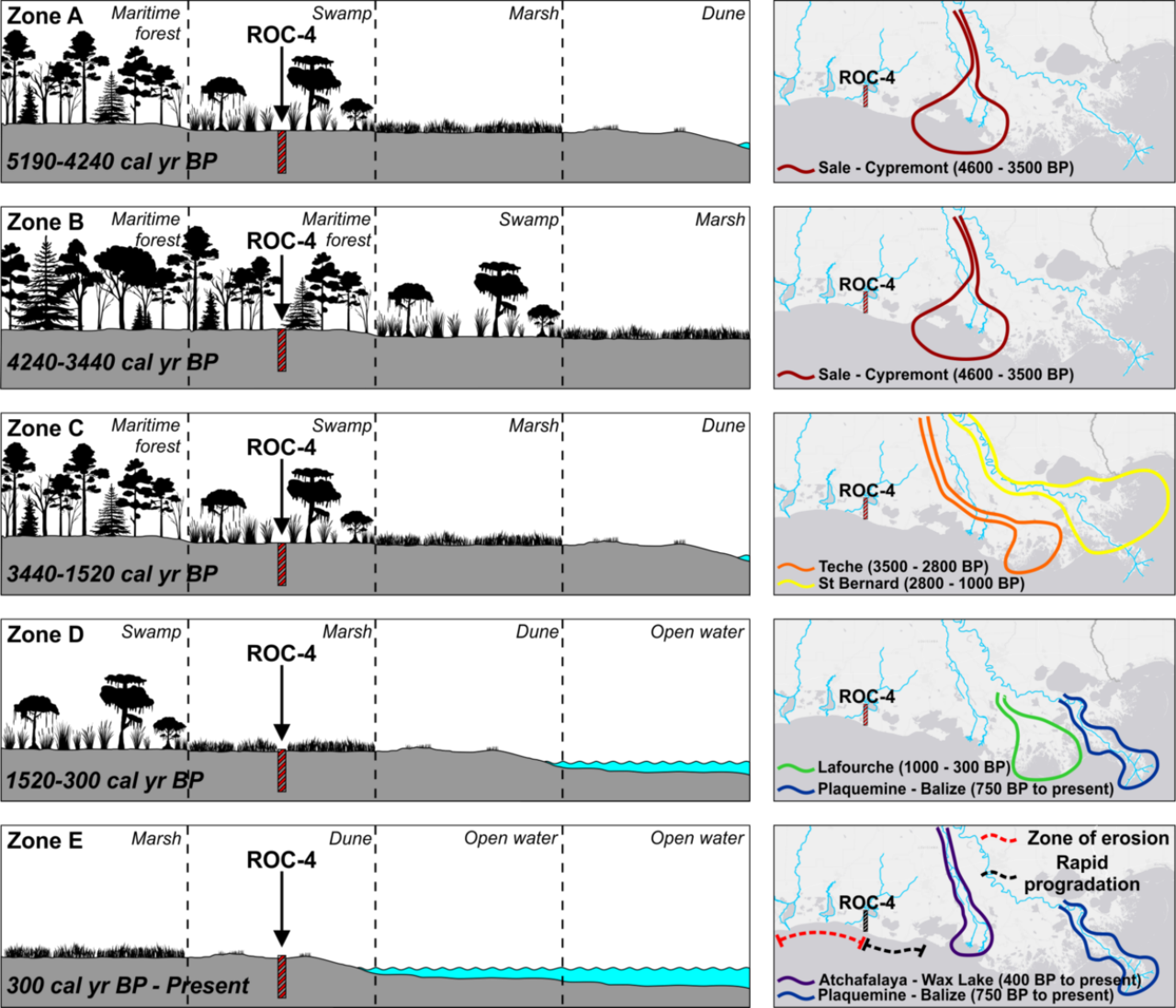
Zone A
Maritime forest
Swamp
Marsh
Dune
ROC-4
5190-4240 cal yr BP
ROC-4
Sale - Cypremont (4600 - 3500 BP)
Zone B
Maritime forest
Maritime forest
Swamp
Marsh
ROC-4
4240-3440 cal yr BP
ROC-4
Sale - Cypremont (4600 - 3500 BP)
Zone C
Maritime forest
Swamp
Marsh
Dune
ROC-4
3440-1520 cal yr BP
ROC-4
Teche (3500 - 2800 BP)
St Bernard (2800 - 1000 BP)
Zone D
Swamp
Marsh
Dune
Open water
ROC-4
1520-300 cal yr BP
ROC-4
Lafourche (1000 - 300 BP)
Plaquemine - Balize (750 BP to present)
Zone E
Marsh
Dune
Open water
Open water
ROC-4
300 cal yr BP - Present
ROC-4
Zone of erosion
Rapid progradation
Atchafalaya - Wax Lake (400 BP to present)
Plaquemine - Balize (750 BP to present)